CERN-ACC-NOTE-2020-0006

17 January 2020
vera.cilento@cern.ch
andrii.pastushenko@cern.ch

ATF2 Ultra-low β_y^* study report for March 2019 run

V. Cilento, CERN, CH-1211 Geneva, Switzerland; Université Paris-Sud, Orsay, France
A. Pastushenko, CERN, CH-1211 Geneva, Switzerland; Université Paris-Sud, Orsay, France
R. Yang, CERN, CH-1211 Geneva, Switzerland
R. Tomás, CERN, CH-1211 Geneva, Switzerland
A. Faus-Golfe, Université Paris-Sud, Orsay, France
N. Terunuma, KEK, Tsukuba, Japan
T. Okugi, KEK, Tsukuba, Japan
K. Kubo, KEK, Tsukuba, Japan

Keywords: CLIC, ATF2, Beam Delivery System, Final Focus System.

Summary

One of the main requests for future linear colliders is to achieve a nanometer vertical beam size at the Interaction Point (IP). Accelerator Test Facility 2 (ATF2) represents a scale down implementation of the final focus system (FFS) concept based to test the novel local chromaticity correction scheme that is implemented in the International Linear Collider (ILC) and the Compact Linear Collider (CLIC) designs. After several years of operations and commissioning, σ_y^* of 41 ± 3 nm was measured at ATF2 with the nominal β_y^* optics in 2016. This paper reports the experimental tuning study done with the ultra-low β_y^* during March 2019 beam operation. This optics has a level of chromaticity comparable with CLIC one and it is expected to reduce σ_y^* below 40 nm.

Contents

1 Introduction

After the discovery of the Higgs boson at the LHC, a lepton based linear collider is considered as one of the potential candidate to continue the high precision particle physics research. In this context, two machines have been proposed to represent the new era of the linear collider research and development platform in the accelerator physics scenario: ILC with a c.o.m. energy of 250 GeV [1] and CLIC with a c.o.m. energy of 380 GeV with a possible upgrade to 3 TeV [2]. These two projects have long linear accelerators that accelerate the particles to high energy and then bring them to collision. Furthermore, the FFS of CLIC and ILC share the same conceptual design based on the local chromaticity correction scheme [3], although the chromaticity level is 5 times higher in CLIC than in ILC (see Table 1). Since this scheme was never used in any accelerator before, a scaled down version of this system was built as a demonstrator in order to prove, experimentally, its effectiveness [4, 5], called ATF2. One of the main goal of ATF2 is to achieve a vertical beam size at the IP of 37 nm. In 2016 an unprecedented vertical beam size at the IP of 41 $\pm$ 3 nm was reached in ATF2 using nominal optics ($10\beta_x^* \times \beta_y^*$) (see fig. 1) [6].

In order to test the feasibility of the FFS local correction scheme with a chromaticity value about a factor 5 higher, like in CLIC, the ultra-low β_y^* optics study has been proposed and studied in ATF2 (see table 1), where the β_y^* value is reduced to 25 μm [7]. The magnetic imperfections and the high order aberrations produced in ATF2 beamline may limit the IP beam size [8]. In order to correct some of these imperfections, a pair of octupoles was installed in 2017 [9] in ATF2 beamline. Different optics are and have been tested in ATF2 such as the nominal one ($\beta_y^* = 100\mu$m), the half β_y^* ($\beta_y^* = 50\mu$m) [6] and the ultra low β_y^* ($\beta_y^* = 25\mu$m) [10, 11]. This report describes the ultra low β_y^* machine study done in March 2019 run.

Table 1: Beam and optics parameters for ILC, CLIC, ATF2 Final Focus Systems.

	ILC	CLIC	ATF2 nominal β_y^* ($10\beta_x^*$ x $1\beta_y^*$)	ATF2 half β_y^* ($10\beta_x^*$ x $0.5\beta_y^*$)	ATF2 ultra-low β_y^* ($25\beta_x^*$ x $0.25\beta_y^*$)
E [GeV]	250	380	1.3	1.3	1.3
L^* [m]	4.1	6	1	1	1
$\epsilon_{y,design}$ [pm]	0.08	0.003	12	12	12
β_x^*/β_y^* [mm]	11/0.41	8/0.1	40/0.1	80/0.05	100/0.025
$\sigma_x^*[\mu m]/\sigma_y^*$[nm]	0.47/5.9	0.149/2.9	8.9/37	8.9/26[a]	12.6/20[a]
$\sigma_{y,meas.}^*$ [nm]	-	-	41$\pm$3	58$\pm$5	64$\pm$3
$\xi_y \approx L^*/\beta_y^*$	10000	50000	10000	20000	40000

[a] Optimized with octupoles.

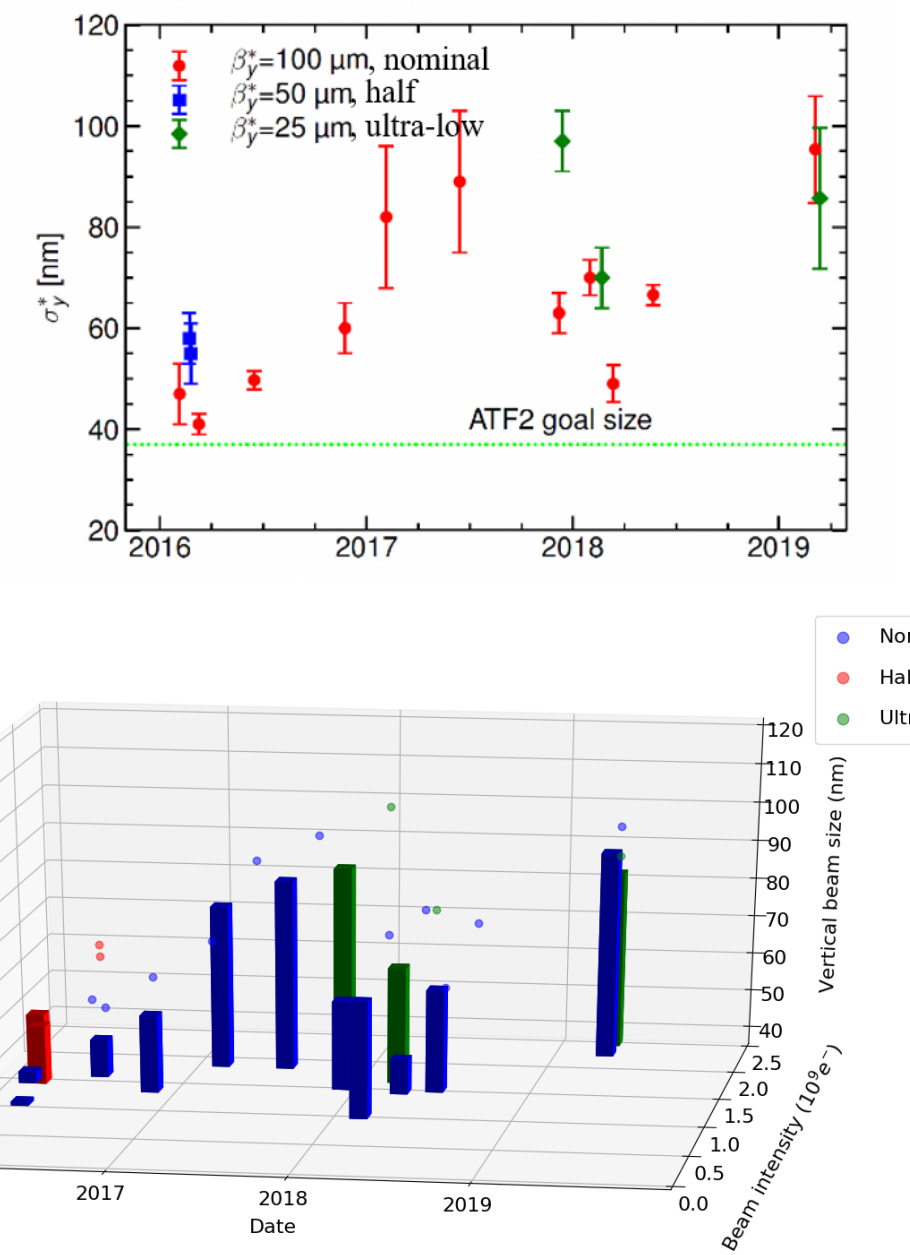

Figure 1: A history of the measured σ_y^* at ATF2 from June 2016 to April 2019. In the bottom plot the beam intensity is also considering as a figure of merit.

2 Experimental study with ultra-low β_y^* optics in ATF2 in March 2019

Following the same tuning procedure used with the half β_y^* optics in [6] in 2016 and following also other tuning studies with the ultra-low β_y^* optics done in December 2017 and February 2018 (see vertical beam size reached in fig. 1) [10, 11], another attempt was done in March

2019 operation with the ultra-low β_y^* optics. A total of 7 shifts (56 hours) have been allocated for the ultra-low β_y^* optics study in March 2019 run. The results of this experimental studies are reported below.

2.1 Complete machine tuning procedure description

In ATF2 before starting any measurement, the machine in tuned to get the desired set-up parameters following this procedure [12]:

1. **Orbit correction**: the beam is steered flat at the BPMs center using the available EXT line correctors and the FFS magnet movers.

2. **Dispersion correction**: dispersion is measured along the FFS by observing the orbit change for the off-momentum beam compared to the on-momentum beam and it is corrected for the horizontal dispersion with QF6X quadrupole, while for the vertical dispersion with a pair of skew quadrupoles QS1X and QS2X.

3. **Coupling correction**: coupling is observed at the entrance of the FFS with m-OTR [12] and it is corrected by minimizing the emittance with Δ-knob and the skew quadrupoles.

4. **Optics matching at the IP**: twiss parameters are measured with the wire scanner and matched to the design values with the matching quadrupoles.

5. **Beam based alignment (BBA)**: each sextupole is aligned with respect to the beam orbit by observing the orbit change on the downstrem BPM.

6. **Beam size tuning**: linear and non linear knobs are combinations of multiple magnets displacements meant to control a chosen set of beam aberrations in order to reach the desired beam size at the IP. They are iteratively used in the tuning process. The IP beam size is measured using the Shintake monitor.

A detailed description of this tuning steps is given below.

2.1.1 Orbit correction

The first step for a correct machine tuning involves the orbit correction in order to reach the best reference orbit possible, called "golden orbit" that corresponds to the orbit with the skew sextupoles aligned in the center (as skew sextupoles are not on movers). The beam orbit diagnostic in the extraction line is handled by 46 beam position monitors (BPMs). There are 13 stripline BPMs, located mainly in the inflector, with a single-shot resolution of about $10\mu m$, 33 C-band cavity BPMs [13], with sub-micron single-shot resolution and 2 button-type BPMs located near the septum [14]. In fig. 2 the position of the skew sextupoles along the beamline is shown. To reach this orbit, some of the ATF2 horizontal and vertical steering magnets are used and the orbit correction is done by changing their currents to minimize the beam offset at the BPMs located along the FF beamline [13]. In fig. 2 we can see an illustration of the orbit during March 2019 beam operation. To be noticed that the last two BPMs around 80 m are not working correctly due to BPM reference signal drifts

and that at the beginning of the EXT line (at around 10 m) there is an orbit bump due to the septum presence and the higher sensitivity of the BPMs in that specific location. The black orbit in fig. 2 represents the difference between the real time orbit and the "golden orbit" and it was quite stable during all March dedicated week for the ultra-low β_y^* study.

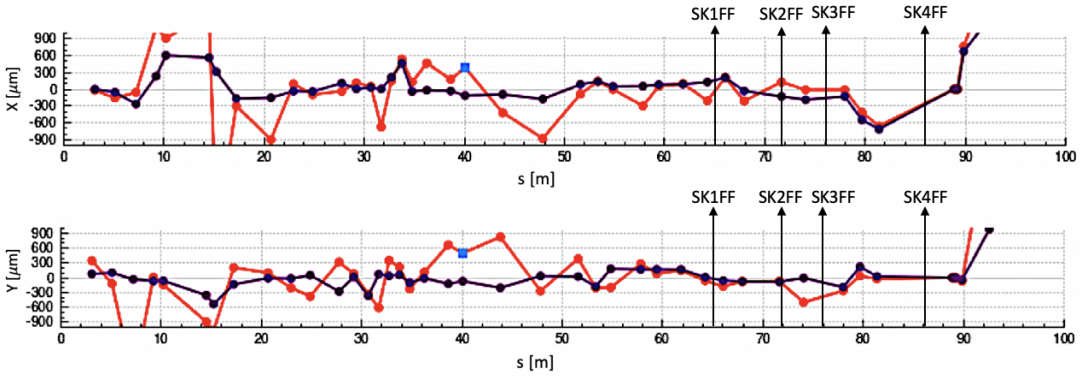

Figure 2: An example of the orbit displayed during March 2019 operation. Red: Real time orbit. Black: difference between the "golden orbit" and the real time orbit.

2.1.2 Dispersion and Coupling correction

After correcting the orbit, dispersion is measured by changing the beam energy in the damping ring and observing the orbit change at the BPMs in the ATF2 beamline. Each measurement involved records the horizontal and vertical position shifts Δx and Δy at the BPMs for different settings of the damping ring rf frequency and fitting linear dependencies to the data to extract the dispersions:

$$D_{x,y} = \frac{\Delta x, y}{\Delta p/p}, \tag{1}$$

where $\Delta p/p$ is the relative momentum shift related to the frequency change Δf by

$$\frac{\Delta p}{p} = -\frac{\Delta f}{f_{DR}} \frac{1}{\alpha}, \tag{2}$$

where $\alpha = 2.14 \times 10^{-3}$ is the momentum compaction factor of the DR. During dispersion measurements the damping ring frequency is changed by ± 2 kHz leading to a relative beam energy change of about $\mp$ 0.13%. The dispersion correction procedure at ATF2 uses quadrupole strength variations. In order to correct the dispersion along the FFS while not affecting too much other parameters, the quadrupoles used for the correction are located at the peaks of dispersion in the extraction line. The vertical dispersion is corrected using a pair of skew quadrupoles QS1X and QS2X that generate vertical dispersion via coupling from the horizontal dispersion. The x, y coupling generated by QS1X is canceled by QS2X thanks to the -I transfer matrix in both planes. The horizontal dispersion is corrected using 2 normal quadrupoles QF1X (located close to QS1X) and QF6X (located close to QS2X). Their strengths

are varied independently until matching the design horizontal dispersion [10]. Figure 3 shows the horizontal and vertical dispersion corrected during March 2019 beam operation.

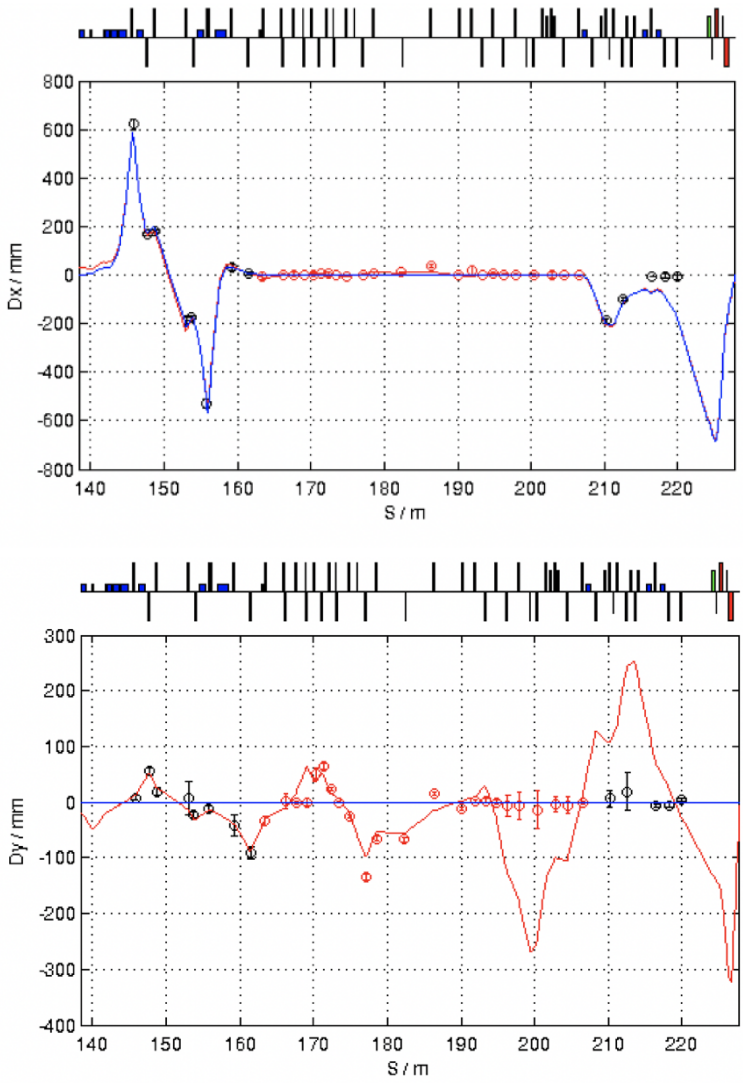

Figure 3: Horizontal (top) and vertical (bottom) dispersion after correction during March 2019 operation. The blue curves represent the design dispersion without machine errors for ATF2 beamline, while the red represents the fit done thanks to the measurements (black points).

2.1.3 Optics Matching at the IP and BBA

The measurements of the $\beta^*_{x,y}$ values are crucial to verify that the desired optics was correctly implemented. The quadrupole scan method is used at ATF2 for the evaluation of the transverse beam parameters. The strengths of the FD quadrupoles QF1FF and QD0FF are scanned while the horizontal and vertical beam size, respectively, are measured using

the IP carbon-wire scanner [15]. In the vincinity of the IP, σ_x and σ_y depend on the beam divergence and waist longitudinal displacement $\Delta f_{x,y}$ according to [10]:

$$\sigma_{x,y}^2 = \epsilon_{x,y}\beta_{x,y}^* + \frac{\epsilon_{x,y}}{\beta_{x,y}^*}\Delta f_{x,y}^2 \tag{3}$$

where the $\beta_{x,y}^*$ are the expected $\beta_{x,y}^*$ at the waist and the measured beam size has to be corrected for residual dispersion at the IP and for the geometric properties of the carbon wire as

$$\sigma_{x,y}^2 = \sigma_{x,y,measured}^2 - \left(\frac{\delta p}{p}\right)^2 \eta_{x,y}^2 - \left(\frac{d}{4}\right)^2. \tag{4}$$

The ATF2 energy spread $\delta p/p$ is 0.6% for low beam intensity of 10^9 e^- bunch and the carbon wire diameter is d = 5 μm. For the horizontal beam size, for which the usual values vary from 6 μm to 10 μm, one can resolve the minimum beam size at the waist so that both emittance and β functions can be determined simultaneously by fitting the parabolic curves to the measured data as a function of the quadrupole magnet current. For the vertical beam size, instead, we expect that it is smaller than 1 μm at the start of the tuning and therefore it cannot be precisely measured at waist with the carbon wire. Only the beam divergence can be measured:

$$\frac{\epsilon_y}{\beta_y^*} = \frac{\sigma_y^2}{\Delta f_y^2}. \tag{5}$$

For a given emittance, one can estimate the vertical beta function at the IP. So the vertical β function is determined by considering the vertical emittance measured upstream the FFS with the m-OTR [16]. During this run we did not evaluate the emittance value at the m-OTR location because of a problem with the vertical dispersion fitting in the software, so the β_y^* value is measured by approximating the emittance in FFS as the one measured in the damping ring (DR).

From the scans in fig. 4 the β functions at the IP have been measured. The β_x^* was 80 $\pm$ 4 mm while the vertical divergence (ϵ_y^* [nm]/β_y^*[mm]) was 0.29 and considering the ϵ_y value the one measured in the DR (ϵ_y = 9.9 pm), the β_y^* was 35 $\pm$ 2 μm with the sextupoles off. The matching of the FFS quadrupoles as well as the sextupole alignment was not performed during the ultra-low β_y^* study. Because of lack of time we used the alignment done during the normal optics operation. Unfortunately, using this alignment that was not very efficient, with the sextupoles on, we had different values of the beta functions since the sextupoles were not well aligned: β_x^* = 120 $\pm$ 4 mm, and β_y^* = 30 $\pm$ 2 μm.

2.1.4 Beam Size Tuning

Shintake monitor for IP Beam Size Measurements

To evaluate the very small vertical beam size at the IP, an interference monitor, where two laser beams cross in the plane transverse to the electron beam in order to form a vertical interference pattern, is used for measuring the vertical beam size at the IP. Such system is called Shintake monitor [17]. The beam size is inferred from the modulation of the resulting

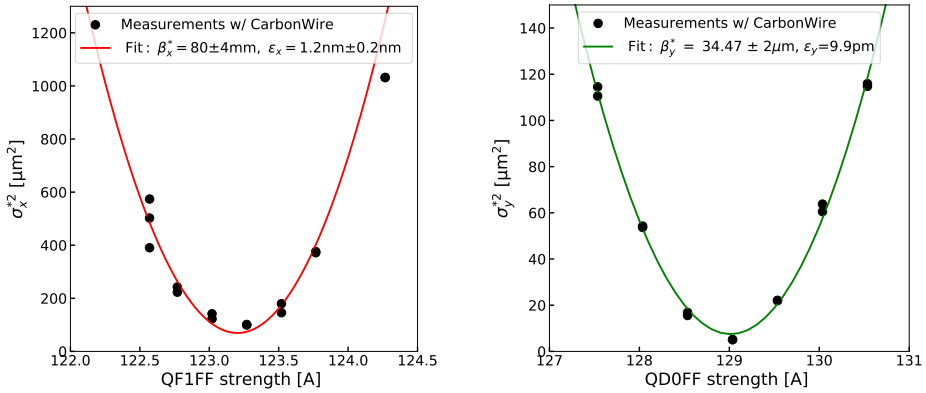

Figure 4: Left: Scan of the square of the horizontal beam size versus QF1FF strength done in March 2019 run. Right: Scan of the square of the vertical beam size versus QD0FF strength scan done in March 2019 run.

Compton scattered photon signal detected by a downstream photon detector. The relation between the beam size and the modulation is the following:

$$\begin{aligned} M &= C\,|\cos\theta|\exp\left[-2(k_y\sigma_y)^2\right], \\ k_y &= \pi/d, \quad d = \frac{\lambda}{2\sin(\theta/2)}, \end{aligned} \tag{6}$$

where C is the modulation reduction factor which represents the overall systematic effect causing a decrease of the observed modulation due to the monitor imperfections , θ is the crossing angle and $\lambda = 532$ nm is the laser wavelength. Three laser crossing angle modes (2-8 degree, 30 degree and 174 degree) extend the beam size measurement range from 5 μm to 20 nm [6]. This relation is essential to better understand the results in the following sections.

In the following section the tuning knobs used in ATF2 are described while the knobs construction for ATF2 ultra-low β_y^* optics is shown in section 3. In section 2.3 a summary of the ultra-low β_y^* tuning done in March 2019 operation is given.

Tuning knobs

In the ATF2 beamline there are 5 normal sextupoles available for the knobs construction, namely SF6, SF5, SD4, SF1 and SD0 and also 4 skew sexupoles, namely SK4, SK3, SK2, SK1 which are available for the aberrations corrections. The linear knobs, that are currently available in the machine and give the best tuning performance are AX knob (horizontal waist shift), AY knob (vertical waist shift), $Coup2$ knob ($y \times x'$ coupling correction), EY knob (vertical dispersion correction). There are also Y_{24} (T^*_{324} term correction) and Y_{46} (T^*_{346} term correction) knobs constructed from the strength variation of the the normal sextupoles and Y_{22} (T^*_{322} term correction), Y_{26} (T^*_{326} term correction), Y_{44} (T^*_{344} term correction) and Y_{66} (T^*_{366} term correction) knobs constructed with the skew sextupoles. From the simulations we know that the most important knobs for the tuning are the waist shift knobs, α_x^*, α_y^*, the vertical dispersion knob D_y^* and the coupling knob $< y, x' >$.

In the tuning process the knobs are applied sequentially, one by one. For each knob scan, the beam size is checked with the Shintake monitor for different knob amplitude. The square of the vertical beam size depends quadratically on the knob amplitude. By fitting σ_y^{*2} with a parabola, it is possible to find the required knob amplitude for the minimum beam size. Ideally after a certain number of iterations we should be able to squeeze the vertical beam size to the design value. A detailed description of the ATF2 tuning knobs is given in [18].

The knobs used during March 2019 ultra-low β_y^* study are AY, EY and $Coup2$, $Y24$ and $Y46$. Figure 5 shows the modulation change when the linear knobs AY, EY and $Coup2$ were used during March beam operation.

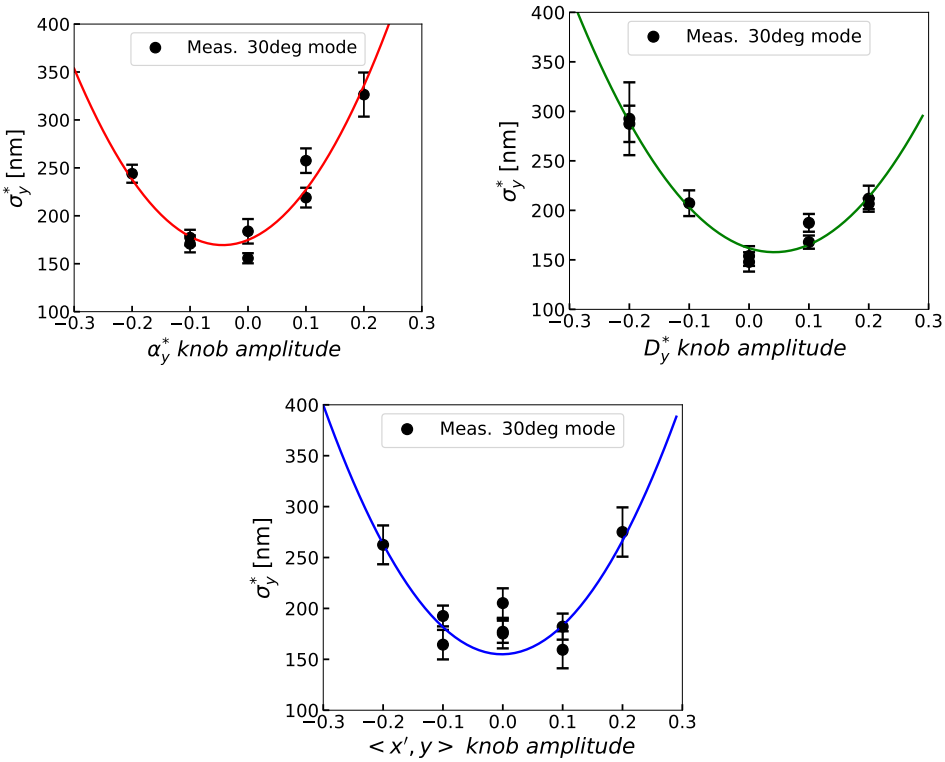

Figure 5: Linear Knobs AY (α_y^*), EY (D_y^*) and $Coup2$ ($< x', y >$) scans done during March 2019 operation at 30 degree mode with the Shintake monitor.

2.2 ATF2 Complementary studies

In some cases some complementary studies have been made:

2.2.1 Energy dependence study

The study of the energy dependence effects on the vertical beam size (defined as df-knob) was for the first time tried with ultra-low β_y^* optics during March 2019 beam operation. From this first attempt with the df-knob, good results can be seen. Smaller beam size (that

means larger M) for higher beam energy can be seen in fig. 6 (for $dE/E \approx 0.1$ % (-2 kHz)). Further study for the energy dependence knob was done during June 2019 beam operation.

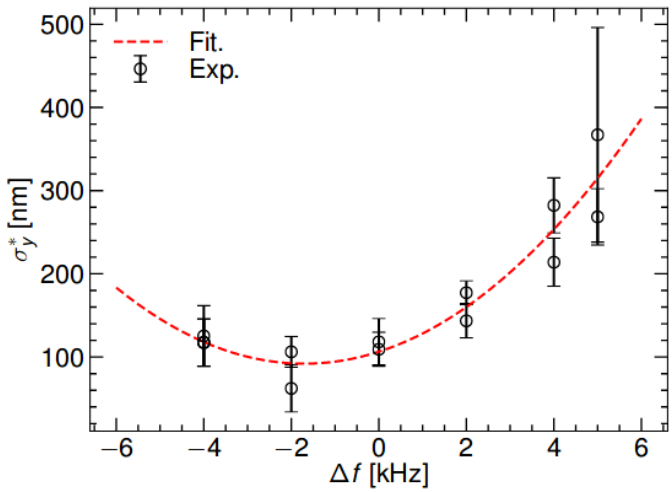

Figure 6: Energy dependence (df-knob) scan done during March 2019 run with the vertical beam size at IP considered as a figure of merit.

2.2.2 ATF2 Octupoles studies

Two octupole magnets were added to the ATF2 beamline in 2017 in order to correct the multipolar field errors [19] and quadrupolar fringe fields [8] in the case of the ultra-low β_y^* optics. The octupole magnets design and manufacturing was done at CERN [9]. One of the octupoles is installed in a dispersive location and the other in a non-dispersive location, with a phase advance of 180^o between them. The proposed and the actual locations for the octupole magnets are: OCT1FF (weaker octupole and the closest to the IP) between QD2AFF and SK1FF and OCT2FF (stronger octupole and furthest to the IP) between QD6FF and SK3FF. The octupoles are expected to be used, when the beam is well tuned in 174 degree mode of the IPBSM, after being properly aligned [10]. The use of the ocupoles was limited during March 2019 beam operation due to the fact that the beam size could not be reduced enough to switch to 174 degree mode.

2.3 Discussion of the results

During March 2019 run 7 shifts in total have been allocated for the ultra-low β_y^* optics study. The first 4 shifts were mostly used to correct the orbit, the dispersion, the coupling and then match the β functions at the IP with the wire scanner (described in section 2.1.3). For a more detailed description of the shifts schedule and actions see table 2. From the $\beta_{x,y}^*$ values with sextupoles on/off, it is clear to see that they were not perfectly aligned. Although the BBA was performed the week before the tuning week study, there was a sextupoles displacement during the beam operation weeks in March 2019.

The rest of the shifts were spent for the beam tuning with IPBSM in 6.4 and 30 degree modes. Unfortunately, 174 degree mode could not be reached in March 2019 operation. The smallest vertical beam size at the IP achieved was 86 ± 14 nm in 30 degree mode (the corresponding modulation was $M \approx 0.76$, see fig. 8) after applying linear and Y_{24} and Y_{46} (see fig. 7) knobs. A summary table of all the relevant parameters during March 2019 run is shown in table 3. Unfortunately, no clear modulation was achieved at 174 degree mode (with $M < 0.1$) since signal found with the Z-scan of the Shintake monitor system. To summarize the tuning of the machine, fig. 7 shows all the knobs applied during March 2019 operation and the respective vertical beam size and modulation reached.

During the 56 hours of tuning, a total of 3 shifts were lost because of several technical issues: a water leak in the septum, IPBSM laser phase module CPU errors, FD mover drifts, EXT orbit and dispersion drifts because of the temperature change and IPBSM modulation was unstable. All these technical problems should be checked carefully before next tuning time beam operation in order to guarantee a better tuning condition for the ultra-low β_y^* study. In the next section dedicated knobs are described in order to improve also the tuning condition of the ultra-low β_y^* study.

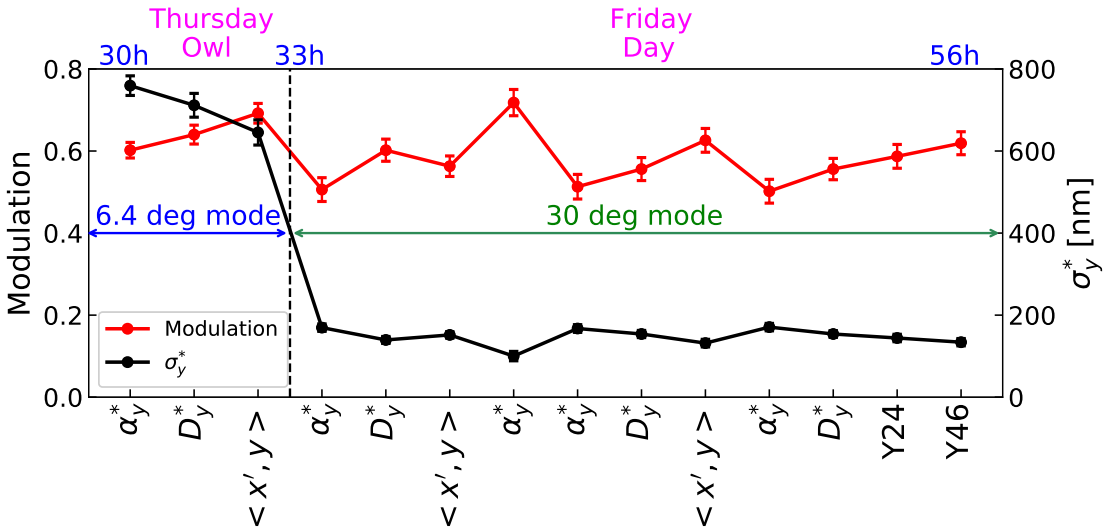

Figure 7: Summary of the modulation (in red) and vertical beam size at the IP σ_y^* (in black) for each knob applied during March 2019 operation.

3 Ultra-low β_y^* Tuning knobs construction using sextupoles

The knobs used during March 2019 ultra-low β_y^* tuning operation were the knobs initially constructed for ATF2 10×1 optics. Although they show a good performance in terms of tuning effectiveness for the ultra-low β_y^* lattice, the knobs specifically constructed for the

Table 2: Summary table of the shifts performed in March 2019 beam operation.

Days	Shifts	Objective	Measured Parameters			
			β_x^* [mm]	ϵ_x^* [nm]	$\frac{\epsilon_y^*[nm]}{\beta_y^*[mm]}$	M
Wed 13/03	Day	Orbit and dispersion correction, EXT orbit and dispersion drifts	-	-	-	-
	Swing	QF1 and QD0 scans w/ sext. off and on, xy coupling correction, set IPBSM for 6.4 deg mode, FFS mover drifts	82.9 79.9 124.3	1.22 1.16 1.07	0.29 0.29 0.32	-
	Owl	QF1 and QD0 scans, no clear modulation at 6.4 degree mode, septum water leak alarm	-	-	-	-
Thu 14/03	Day	Restart of operation after the water leak, radiation alarm interlock, modulation recovery at 6.4 deg mode, QDO mover problem, phase module system error	96.8	1.56	0.42	-
	Swing	IPBSM problem fixed, clear modulation was found at 6.4 deg mode	-	-	-	-
	Owl	Linear knobs scans at 6.4 deg mode, set IPBSM for 30 deg mode	-	-	-	0.7 (at 6.4 deg mode)
Fri 15/03	Day	Beam size tuning at 30 deg mode, energy dependence study	-	-	-	0.75 (at 30 deg mode)
	Swing	set IPBSM for 174 deg mode, no clear modulation was found, beam off at 19:20	-	-	-	-

Table 3: Summary table of the relevant parameters during March 2019 beam operation.

M	β_x^*[mm]	$\beta_y^*[\mu$m]	$\sigma_x^*[\mu$m]	σ_y^*[nm]	ϵ_x^*[nm]	ϵ_y^*[pm]
0.76 ± 0.03	80 ± 4	35 ± 2	9.8 ± 1.1	86 ± 14	1.2 ± 0.2	9.9 (DR)

ultra-low β_y^* would shorten the tuning time. In preparation of the next run of the ultra-low β_y^* study, dedicated knobs are constructed and described in the following sections.

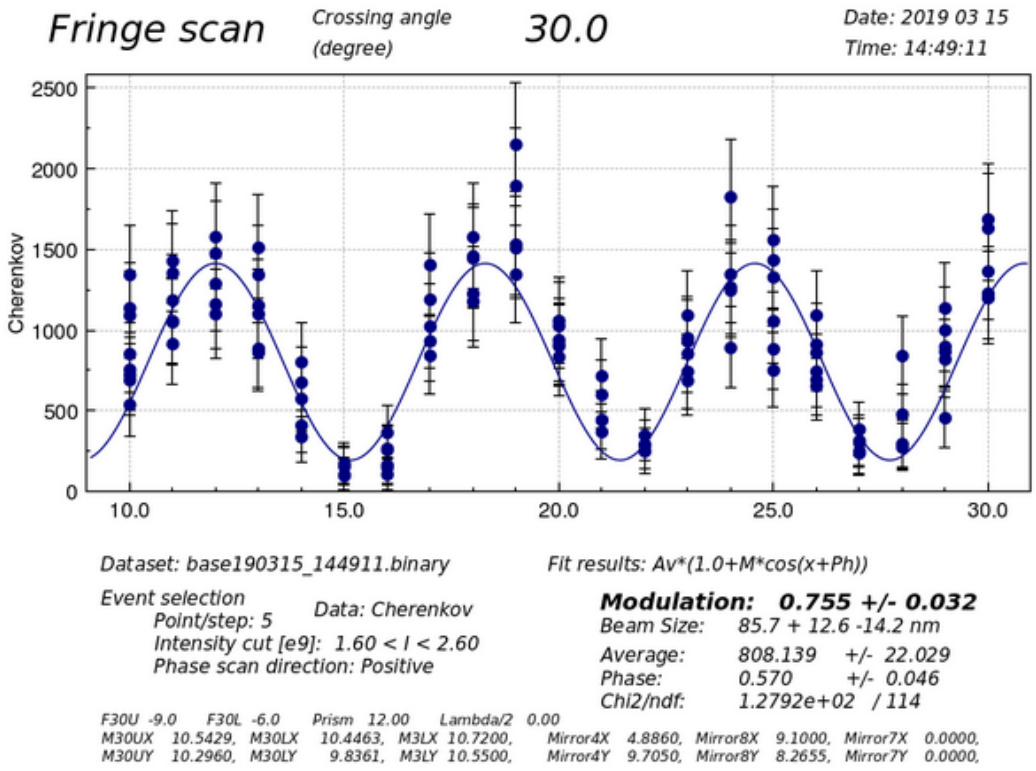

Figure 8: Fringe scan for the smallest vertical beam size ($\sigma_y^* = 86 \pm 14$ nm) achieved at ATF2 during March 2019 operation.

3.1 Knobs definition

To describe the beam dynamics in the FFS, Taylor map formalism is used [20]. It is modified in a way to connect the measured beam size with the aberrations observed at the IP. Vertical position at the IP reads as:

$$y^* = y_0 + \sum_{i=1}^{6} R_{3i}^* u_i^* + \sum_{i=1}^{6}\sum_{j=1}^{6} T_{3ij}^* u_i^* u_j^* + ..., \tag{7}$$

y_0 is betatron coordinate of the particle, $y_0 = \sqrt{\epsilon\beta}\sin(\Psi)$ and $u^* = (x^*, x'^*, y^*, y'^*, \delta)$ is the vector of the particle's coordinates at the IP. Vertical beam size is the following:

$$\sigma_y^{*2} = \epsilon_y\beta_y^* + \sum_{i=1}^{6} R_{3i}^* < y^*, u_i^* > + \sum_{i=1}^{6} T_{3ij}^* < y^*, u_i^*, u_j^* > + ... \tag{8}$$

For the perfect machine, the contributions from any terms, except $\epsilon_y\beta_y^*$, are small. In reality, these terms are no longer negligible in the presence of different imperfections. To correct lattice errors, especially at the IP, a set of orthogonal knobs has been constructed for ultra-low β_y^* optics [18], aiming to reduce the impact from one particular term on the beam size. When a normal sextupole is moved horizontally, a normal quadrupole field is generated, when it is moved vertically, skew quadrupole field is generated. The strengths of such fields

depends on the corresponding shift and this will impact: the horizontal and vertical IP alpha functions (α_x^*, α_y^*), the horizontal dispersion (D_x^*) and the first derivative of the horizontal dispersion (D'^*_x) for horizontal movement and vertical dispersion (D_y^*), the first derivative of the vertical dispersion (D'^*_y) and the coupling components between x and y plane such as $< y, x >$ and $< y, x' >$. From the simulations, the conditions between the sextupoles shifts are established to allow to change each specific value at the IP almost independently of the others and such a knob is called orthogonal.

These knobs are constructed in the following way. A knob for a vertical beam size to correct the coupling with the coordinate u^i:

$$R_{3i}^{knob} = \frac{< y, u^i >}{\sigma_y \sigma_{u^i}} \tag{9}$$

Nonlinear knobs are constructed by varying the strength of the sextupoles available in the FFS, either normal or skew sextupoles. They are constructed in the same way as the linear knobs. For the coupling with coordinates u^i and u^j knobs are defined as:

$$T_{3ij}^{knob} = \frac{< y, u^i, u^j >}{\sigma_y \sigma_{u^i} \sigma_{u^j}} \equiv Y_{ij} \tag{10}$$

3.2 Knobs construction

The knobs are defined as shown in Eq. (9), (10). In order to construct them orthogonally, one has to evaluate the response matrix based on these knobs assuming a linear change of the corresponding knobs. First, we start with the linear knobs, constructed from the horizontal shifts of the normal sextupoles. The response matrix for the vector of shifts $(x_1, x_2, x_3, x_4, x_5)$ (they are assumed to be small) of 5 normal sextupoles is based on the Sigma matrix at the IP [21]:

$$\begin{bmatrix} \frac{d}{dx_1} < x, x > & \frac{d}{dx_2} < x, x > & \dots & \frac{d}{dx_5} < x, x > \\ \frac{d}{dx_1} < x, x' > & \frac{d}{dx_2} < x, x' > & \dots & \frac{d}{dx_5} < x, x' > \\ \dots & \dots & \dots & \dots \\ \frac{d}{dx_1} < z, z > & \frac{d}{dx_2} < z, z > & \dots & \frac{d}{dx_5} < z, z > \end{bmatrix} \tag{11}$$

The shifts are applied independently one from another in an error free lattice. One can also extract the interesting terms from this matrix and form the matrix of a smaller rank, but has to be aware of the other terms, because when the knobs are not constructed properly, they may contribute to the terms not taken into account initially. For example, the matrix has following structure for the α_x^*, α_y^* and D_x^* knobs:

$$\begin{bmatrix} \frac{d}{dx_1} < x, x' > & \frac{d}{dx_2} < x, x' > & \dots & \frac{d}{dx_5} < x, x' > \\ \frac{d}{dx_1} < y, y' > & \frac{d}{dx_2} < y, y' > & \dots & \frac{d}{dx_5} < y, y' > \\ \frac{d}{dx_1} < x, \delta > & \frac{d}{dx_2} < x, \delta > & \dots & \frac{d}{dx_5} < x, \delta > \end{bmatrix} \tag{12}$$

In order to get the orthogonal basis for the the sextupoles shifts, one has to use the SVD to factorize the response matrix $R = USV^T$. The rows of matrix V^T are than taken as the knobs.

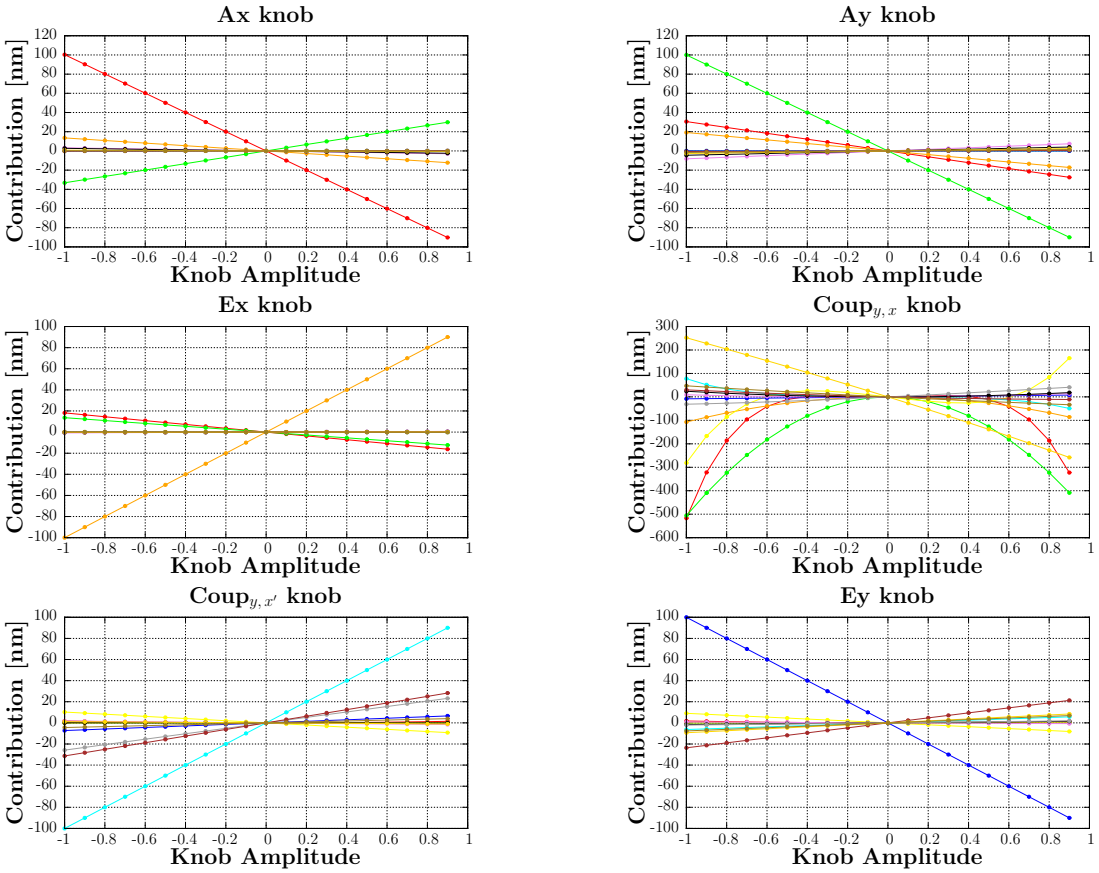

Figure 9: Vertical beam size contributions from linear knobs:
| — **Ax** | — **Ay** | — **Ex** | — **Coup**$_{y,x}$ | — **Coup**$_{y,x'}$ | — **Ey** |

The rest of the knobs follow the same construction strategy. We construct the linear knobs $< y, x >$, $< y, x' >$ and D_y^* using the vertical shifts of the normal sextupoles, the nonlinear knobs Y_{24} and Y_{46} by varying the strength of the normal sextupoles and the Y_{22}, Y_{26}, Y_{44} and Y_{66} knobs by varying the strength of four skew sextupoles.

3.3 Orthogonality validation of the ultra-low β_y^* optics knobs

To validate whether the constructed knobs are orthogonal or not, one has to apply the knob and check the different contributions to the beam size. If it is constructed properly, the largest term, generated by applying the knob on error-free lattice should correspond to the knob applied. One can get the beam size contribution associated with the linear knob R_{3i}^{knob}, for example, from Eq. (8) by putting $R_{3i}^* = \frac{<y^*,u_i^*>}{<u_i^*,u_i^*>}$:

$$P(R_{3i}^{knob}) = \frac{< y, u_i^* >}{\sigma_{u_i^*}} \tag{13}$$

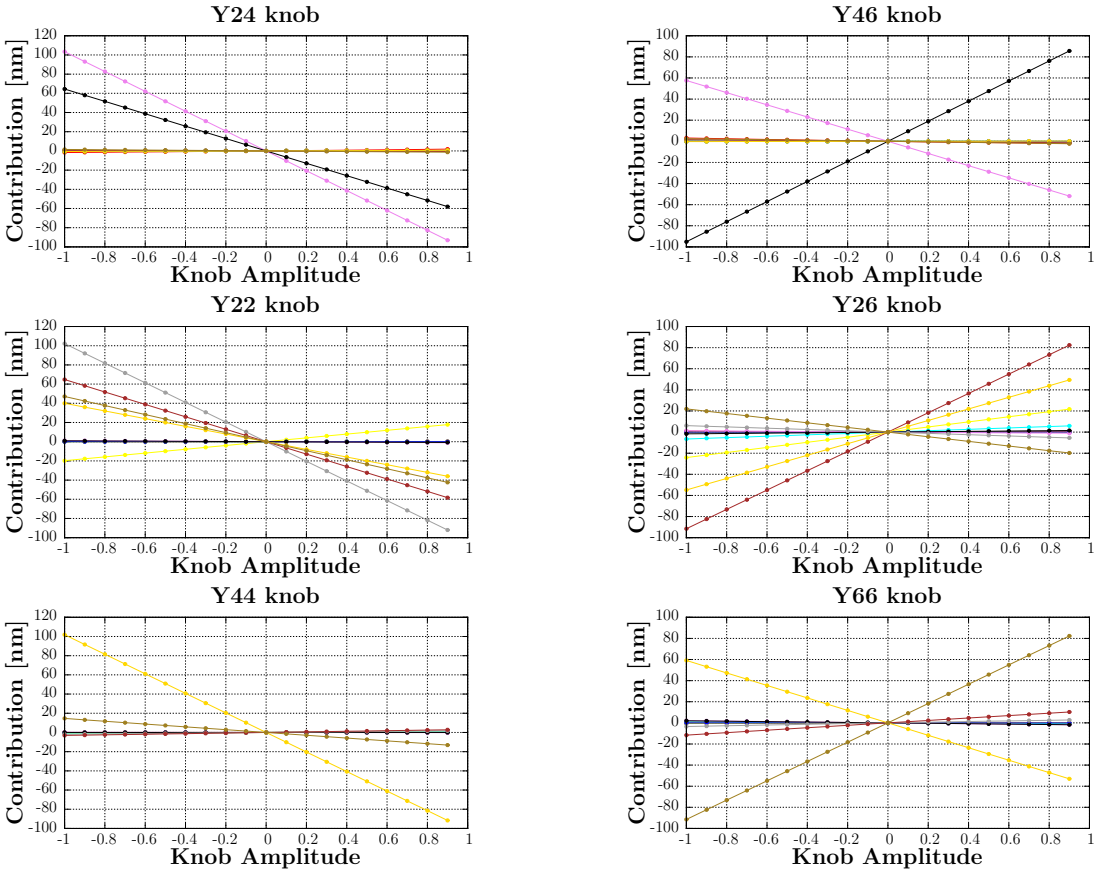

Figure 10: Vertical beam size contributions from nonlinear knobs:
| — **Y24** | — **Y46** | — **Y22** | — **Y26** | — **Y44** | — **Y66** |

All the contributions are squared in the beam size equation:

$$< y^*, y^* >= \epsilon_y \beta_y^* + \sum_{i=1}^{6} (P(R_{3i}^{knob}))^2 + \sum_{i,j=1}^{6} (P(T_{3ij}^{knob}))^2 + ... \tag{14}$$

The orthogonality properties of all the constructed knobs for the ultra-low β_y^* optics (25 $\beta_x^* \times$ 0.125 β_y^*) is shown in figs. 9, 10 . Satisfactory orthogonality properties were observed for most of them, except for the $\text{Coup}_{y,x}$ knob, where strong nonlinearities are simulated, so a further study is still needed to improve the performance of this knob.

4 Conclusion and Future Work

During March 2019 the ultra-low β_y^* optics was well matched and the twiss parameters at the IP were well approximated to the design values, but unfortunately, the run ended with an incomplete machine tuning because of some technical problems that turned out to be the main limitations for reaching a very small vertical beam size at the IP.

A whole week in June 2019 beam operation has been allocated for the ultra-low β_y^* for future studies. The main goal of the future ATF2 studies will be firstly to recover the

performance of the IPBSM at 174 degree mode with the nominal optics 10×1. During next beam operations there will be also the chance to use the DFS with the ultra-low β_y^* optics and there will be also the opportunity to perform the octupoles alignment and to clarify the octupoles role in the tuning process.

Regarding the ultra-low β_y^* tuning knobs, future plans will involve simulation studies to better understand the potential of the knobs specifically constructed for the ultra-low β_y^* optics and what is the gain they can provide in the terms of tuning effectiveness compared to the knobs presently used on ATF2.

Acknowledgements

Many thanks to all ATF2 collaborators for the help and the support during this tuning study.

References

[1] Philip Bambade, Tim Barklow, Ties Behnke, Mikael Berggren, James Brau, Philip Burrows, Dmitri Denisov, Angeles Faus-Golfe, Brian Foster, *et al.* "The International Linear Collider. A Global Project". March 2019. arXiv:1903.01629v3.

[2] A. Robson, P.N. Burrows, N. Catalan Lasheras, L. Linssen, M. Petric, D. Schulte, E. Sicking, S. Stapnes, W. Wuensch. "The Compact Linear e+ e- Collider (CLIC): Accelerator and Detector". Dec. 2018. arXiv:1812.07987.

[3] P. Raimondi, A. Seryi. "Novel final focus design for future linear colliders". Physical review letters, 2001, 86.17: 3779.

[4] K. Kubo, et al. "Extremely low vertical-emittance beam in the Accelerator Test Facility at KEK." Physical review letters 88.19 (2002): 194801.

[5] G. R. White et al. "Experimental Validation of a Novel Compact Focusing Scheme for Future Energy-Frontier Linear Lepton Colliders". Phys. Rev. Lett. 112 (2014).

[6] M. Patecki, D. Bett, E. Marin, F. Plassard, R. Tomás, K. Kubo, S. Kuroda, T. Naito, T. Okugi, T. Tauchi and N. Terunuma. "Probing half β_y^* optics in the Accelerator Test Facility 2". Physical Review Accelerators and Beams, 19(10), 101001 (2016).

[7] E. Marin et al. "Design and high order optimization of the Accelerator Test Facility lattices". Phys. Rev. ST Accel. Beams 17 (2014).

[8] M. Patecki and R. Tomás. "Effects of quadrupole fringe fields in final focus systems for linear colliders." Physical Review Special Topics-Accelerators and Beams 17.10 (2014): 101002.

[9] E. Marin, M. Modena, T. Tauchi, N. Terunuma, R. Tomás, GR. White, et al. "Specifications of the octupole magnets required for the ATF2 ultra-low β_y^* lattice". Tech. rep. SLAC National Accelerator Laboratory (SLAC), 2014.

[10] F. Plassard. "Optics optimization of longer L* Beam Delivery System designs for CLIC and tuning of the ATF2 final focus system at ultra-low β_y using octupoles". No. CERN-THESIS-2018-223. HAL, 2018.

[11] V. Cilento. "Optimization of the Beam Size at the Interaction Point of the Accelerator Test Facility 2". CERN-THESIS-2018-191. Master Thesis. Universita del Sannio (IT).

[12] G. White, A. Seryi, M. Woodley, E. Marin, Y. Kamiya, S. Bai, B. Bolzon, K. Kubo, S. Kuroda, T. Okugi, et al. "Operational Experiences Tuning the ATF2 Final Focus Optics Towards Obtaining a 37 nm Electron Beam IP Spot Size". 1st International Particle Accelerator Conference (IPAC 2010). Joint Accelerator Conferences Website. 2010, pp. 2383 - 2385.

[13] Y.I. Kim, R. Ainsworth, A. Aryshev, ST. Boogert, G. Boorman, J. Frisch, A. Heo, Y. Honda, W.H. Hwang, J.Y. Huang, et al. "Cavity beam position monitor system for the Accelerator Test Facility 2". Physical Review Special Topics-Accelerators and Beams 15.4 (2012), p. 042801.

[14] Marcin Patecki. "Optimisation analysis and improvement of the effective beam sizes in Accelerator Test Facility 2". PhD thesis. Warsaw University of Technology (PL), 2016.

[15] S. Bai, A. Aryshev, P. Bambade, D. Mc Cormick, B. Bolzon, J. Gao, T.Tauchi and F. Zhou. "First beam waist measurements in the final focus beamline at the kek accelerator test facility 2". Phys. Rev. ST Accel. Beams 13, 092804, 2010.

[16] J. Alabau-Gonzalvo, C. Blanch Gutierrez, A. Faus-Golfe, J.J. Garcia-Garrigos, J. Resta-Lopez, J. Cruz, D. McCormick, G. White, and M. Woodley. "The ATF2 Multi-OTR System: Studies and Design Improvements". International Beam Instrumentation Conference. 2012.

[17] T. Shintake, D. Walz, A. Hayakawa, M. Ohashi, K. Yasuda, D. Burke, S. Wagner, Y. Ozaki, and H. Hayano. "Design of laser Compton spot size monitor". Int. J. Mod. Phys. Proc. Suppl. 1.KEK-PREPRINT-92-65 (1992), pp. 215-218.

[18] T. Okugi, S. Araki, P. Bambade, K. Kubo, S. Kurado, M. Masuzawa, E. Marin, T. Naito, T. Tauchi, N. Terunuma, et al. "Linear and second order optics corrections for the KEK Accelerator Test Facility final focus beam line". Physical Review Special Topics-Accelerators and Beams 17.2 (2014), p. 023501.

[19] Fabien Plassard, Andrea Latina, Eduardo Marin, Rogelio Tomás, and Philip Bambade. "Quadrupole-free detector optics design for the Compact Linear Collider final focus system at 3 TeV". In: Phys. Rev. Accel. Beams 21 (1 Jan. 2018).

[20] Brown, Karl L. "A First and Second Order Matrix Theory for the Design of Beam Transport Systems and Charged Particle Spectrometers". Adv. Part. Phys., volume 1, 1968, 71-134, SLAC-75.

[21] J. Ogren, A. Latina, R. Tomás and D. Schulte. "Tuning of the CLIC 380 GeV Final-Focus System with Static Imperfections". CERN, Geneva, CERN-ACC-2018-0055. CLIC-Note-1141, Dec. 2018.